

See discussions, stats, and author profiles for this publication at: <http://www.researchgate.net/publication/272640570>

# Regional implications of U-Pb zircon ages from rhyolitic pebbles of Suncho Formation conglomerates, northern Sierras Pampeanas (NW Argentina)

ARTICLE *in* NEUES JAHRBUCH FÜR GEOLOGIE UND PALÄONTOLOGIE - ABHANDLUNGEN · JANUARY 2015

Impact Factor: 0.52 · DOI: 10.1127/njgpa/2015/0447

---

READS

65

## 5 AUTHORS, INCLUDING:



Alejandro J. Toselli

National University of Tucuman

77 PUBLICATIONS 764 CITATIONS

[SEE PROFILE](#)



Guillermo F. Aceñolaza

National University of Tucuman

45 PUBLICATIONS 218 CITATIONS

[SEE PROFILE](#)



Miguel Basei

University of São Paulo

178 PUBLICATIONS 1,764 CITATIONS

[SEE PROFILE](#)



Florencio G. Aceñolaza

National University of Tucuman

30 PUBLICATIONS 354 CITATIONS

[SEE PROFILE](#)



## Regional implications of U-Pb zircon ages from rhyolitic pebbles of Suncho Formation conglomerates, northern Sierras Pampeanas (NW Argentina)

Alejandro J. Toselli, Guillermo F. Aceñolaza, Miguel A. Basei, Florencio Aceñolaza,  
and Juana N. Rossi

With 5 figures and 2 tables

**Abstract:** Conglomerates are scarce in the Neoproterozoic/Cambrian strata of the South American Central Andean Basin. In NW Argentina, unusual conglomerates within meta-psammites of the Suncho Formation contain rhyolite clasts that yielded  $524.9 \pm 1.12$  Ma and  $525.1 \pm 1.3$  Ma LA-ICP-MS U-Pb zircon ages. These ages coincide with the reported youngest age populations obtained from detrital zircons in the host rocks. The new geochronological data, the regional geology and published data suggest that the source areas of these pebbles were located to the NE and E of the Suncho Formation, which may include some reworked older sedimentary levels of the Puncoviscana Formation. The origin of the Suncho conglomerate is linked to Pre-Tilcaric magmatism which closed the Pampean Cycle, whose ages are in the range 541–517 Ma. The match between the radiometric data and the age provided by the *Oldhamia* trace fossils with both sedimentary and magmatic events occurring during the Terreneuvian – Series 2 time span (“lower Cambrian”) is here emphasized. Considering that the dated rhyolite clasts were derived from magmatic rocks, a Puncoviscana active margin can be proposed as their source, and an active margin setting is proposed for Puncoviscana in this part of the western margin of South America.

The knowledge of unusual facies within the Neoproterozoic/Cambrian sequences in the South American Andes provides a better understanding of the geology of little known areas in the western proto-gondwanan margin.

**Key words:** Rhyolite pebbles, Cambrian conglomerates, Provenance, Suncho Formation, NW Argentina.

### 1. Introduction

The Sierra de la Ovejería represents an important orographic unit of the Pampean Ranges (NW Argentina), and is characterized as a fault-bounded block in the southern branch of the Aconquija Range.

GONZALEZ BONORINO (1950) and DURAND (1980) provided the first detailed data on the stratigraphy and the geological outline of the region. ACEÑOLAZA & TOSELLI (1978) correlated the Suncho Formation with the Puncoviscana Formation by comparing lithology and trace-fossil associations from both units.

DURAND (1985) described a polymictic conglomerate and named it El Medano Member, which includes rounded clasts of quartzites, greywackes, sandstones, limestones and rhyolite pebbles. DURAND (1985) also argued that the conglomerates occur as local intercalations in the turbidite sequence of the Suncho Formation, and interpreted them as mud-supported turbidity currents and debris flows.

Even though they show incipient metamorphism, rocks still display remarkable primary sedimentary structures such as well-defined bedding planes bearing trace fossil associations characterized by *Old-*

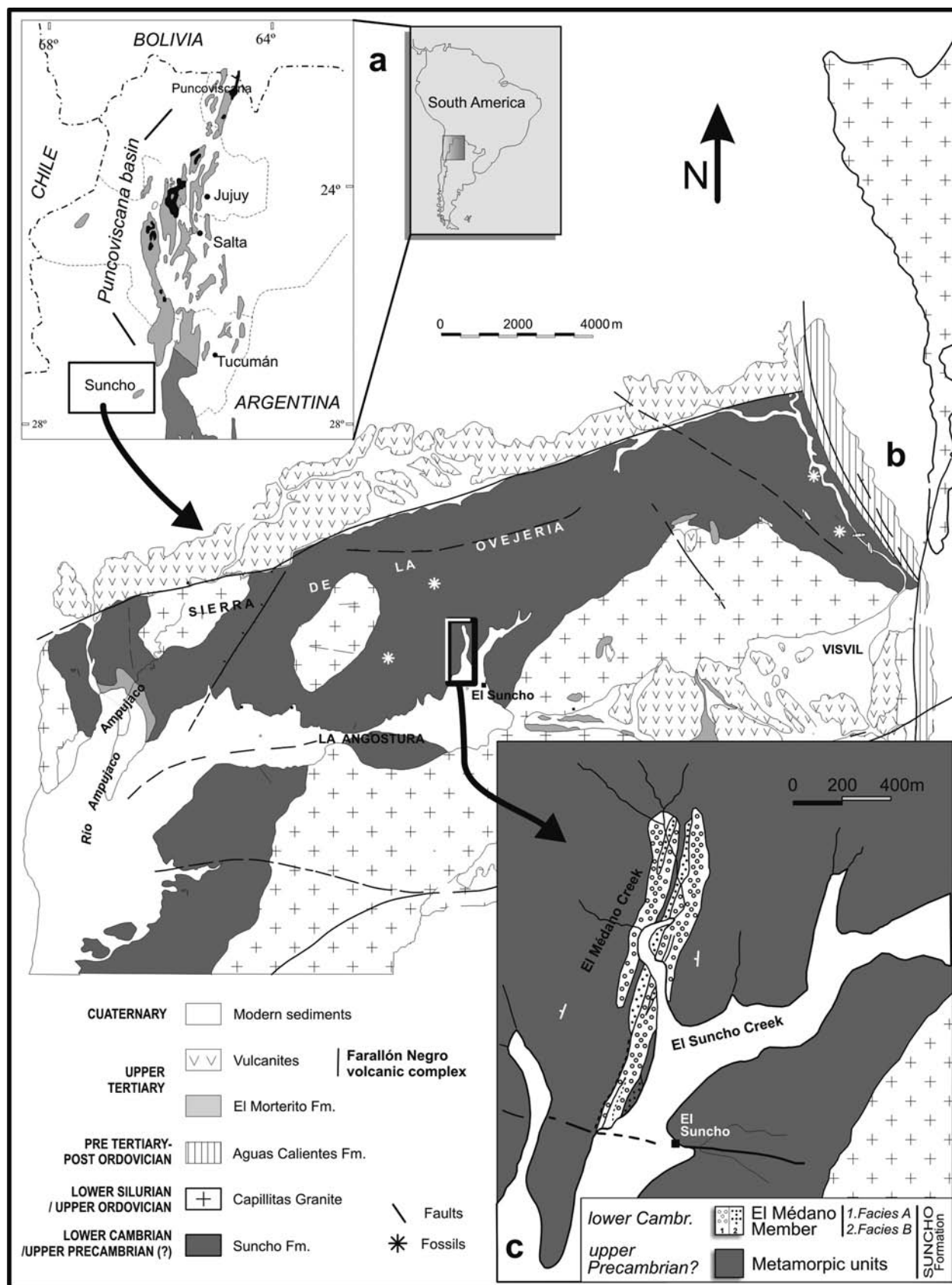
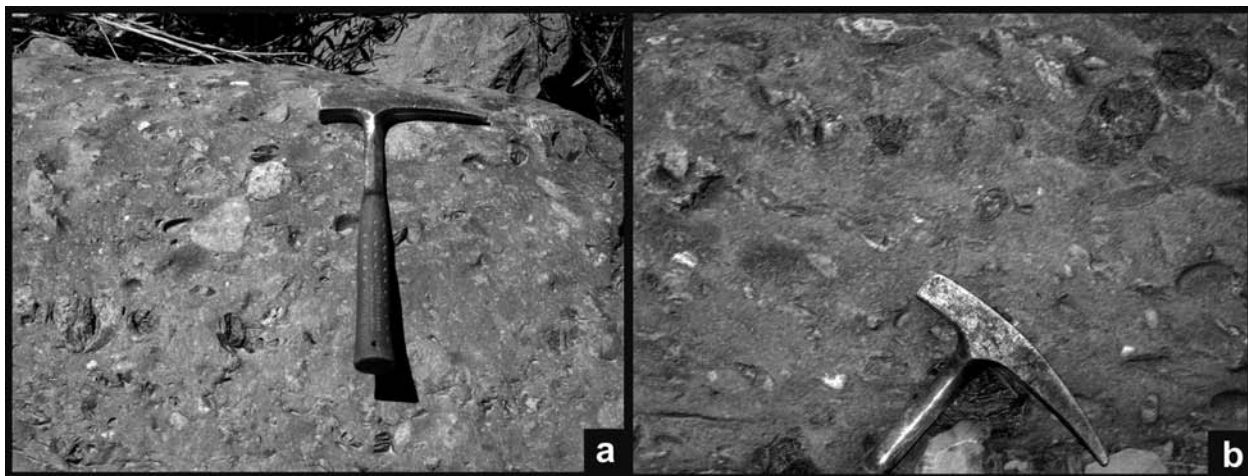


Fig. 1.



**Fig. 2.** Conglomerates of the Suncho Formation cropping out in the Quebrada del Médano (Catamarca, NW Argentina).

*hamia* isp. This suggests a Terreneuvian age for the sequence (“Lower Cambrian”) as stated by MIRRÉ & ACEÑOLAZA (1972). The sedimentary rocks are mainly represented by metawacke lithofacies, arranged mostly as 50 cm thick beds with sporadic shaly intercalations containing the Terreneuvian-aged trace fossils (DURAND 1985).

Geochronological data on the detrital zircons of the Suncho Formation psammites display Meso-Proterozoic and Early Neoproterozoic ages, with a major age abundance peak between 552 and 514 Ma (U-Pb ages; ADAMS et al. 2011).

The purpose of this research is to pin-point the age of rhyolite clasts in the conglomerates of the Suncho Formation, and to address the relation of these magmatic rocks with the important orogenic event (Tilcaric phase) during the Ediacaran to Early Cambrian. These will enhance the understanding of one of the most important Neoproterozoic / Early Paleozoic basins in the Central Andes, the Puncoviscana Basin.

## 2. Geological setting

The Suncho Formation crops out in the Sierra de La Ovejería and is generally considered as a sequence in association with the Puncoviscana Basin based on

common geological, petrographic and paleontological signatures (Fig. 1A). A regional interpretation of the Suncho Formation is difficult due to limited exposure, the lack of a known stratigraphic basement and the deformation affecting the sequences. The only clear geological data on the stratigraphy of the unit is given by the Ordovician Capillitas granite intruding the whole sequence (RAPELA et al. 1999 reported ages of  $470 \pm 3$  Ma by U-Pb SHRIMP on zircon), and the Tertiary strata unconformably overlying it. The age of sedimentation, based on trace-fossil associations with the notable *Oldhamia* isp., was established by DURAND (1980) as early Cambrian (Terreneuvian – Series 2).

Low grade metaconglomerates and shales with preserved sedimentary structures were described by DURAND (1982) as the typical facies of the unit. Undulate current ripple marks are common in the sequence. Subsequent deformations have generated two main oblique cleavage planes displaying chlorite and illite as index minerals, denoting the transition from anchizone to greenschist-facies metamorphism.

The conglomerates of the El Medano Member, which are intercalated with meta-psammites of the Suncho Formation, form a NNE-SSW oriented elongate outcrop about 1200 m long and 200 m wide, and have a maximum thickness of about 150 m (Fig.

**Fig. 1.** A – Location and distribution of outcrops in the Puncoviscana Basin, NW Argentina. B – Geological sketch map of the Sierra de la Ovejería, Catamarca Province, NW Argentina (modified from DURAND 1980). C – Quebrada de Suncho locality (modified from DURAND 1985).

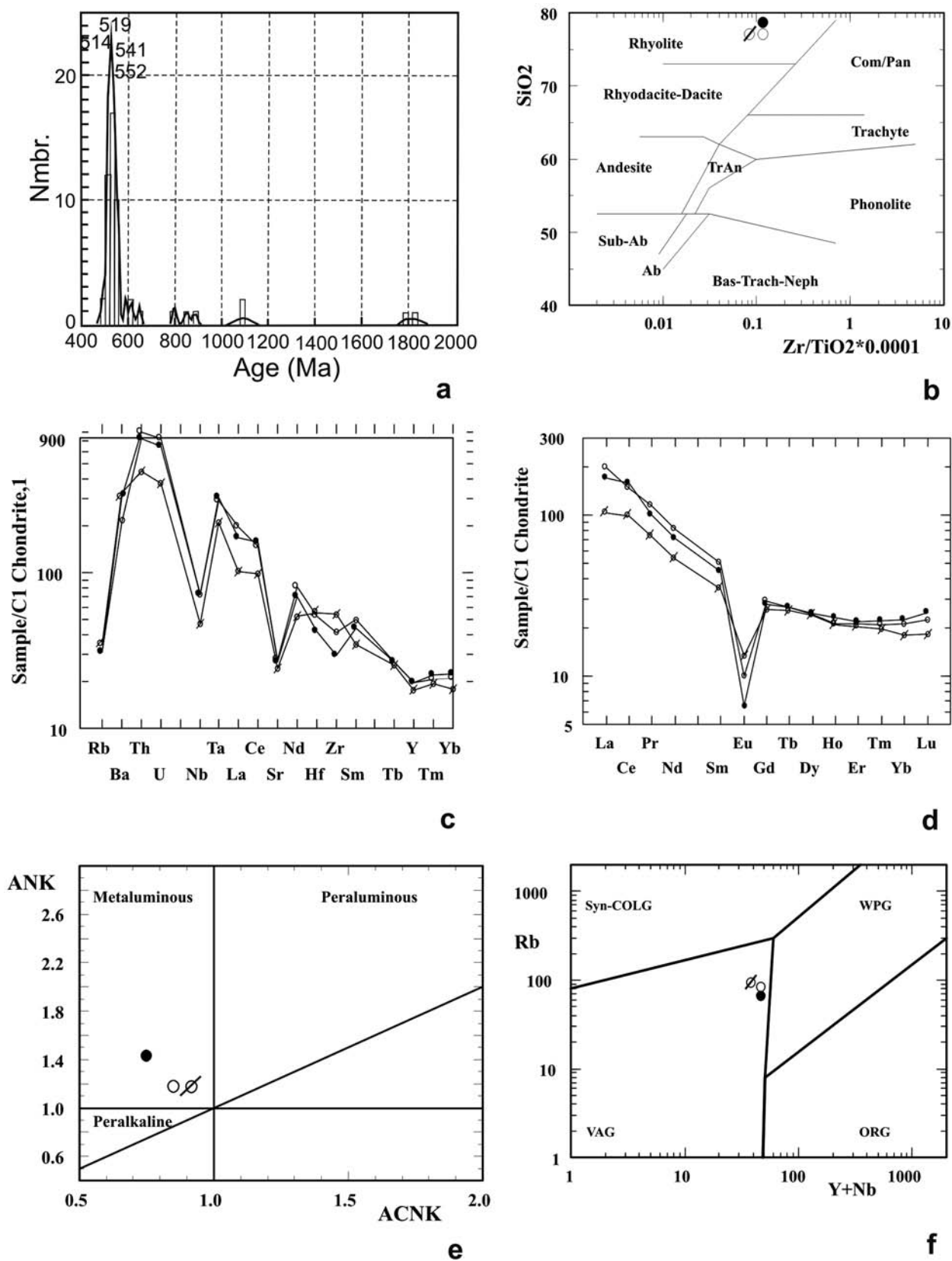


Fig. 3.

1B-C). The conglomerates have also been metamorphosed, and are characterized by subrounded clasts more or less dispersed in a dominant psammo-pelitic matrix. The pebbles have average diameters of 4 to 6 cm and consist of sandstones, greywackes, quartzites, limestones and rhyolites, defining a polymictic conglomerate (Fig. 2).

Detailed sampling of volcanic pebbles was performed for the conglomerate facies of the Suncho Formation along the Suncho Creek (Fig. 1). Forty-nine fragments were obtained and used for macroscopic and microscopic petrographic characterization. Among them, twelve rhyolite fragments were chosen for geochemical and chronological analyses after mechanical reduction and homogenization of samples. The geological characters of outcrops, the narrow spread of the U/Pb zircon ages, and the petrographical and geochemical homogeneity point to a single source for the rhyolite clasts. The detrital zircon population of the metasedimentary rocks unit has Mesoproterozoic and early Neoproterozoic U-Pb ages, with a significant peak between 552 and 514 Ma., in concordance with the data obtained by ADAMS et al. (2011) (Fig. 3A).

### 3. Petrography of rhyolites

Rhyolite clasts from the El Médano Member of the Suncho Formation were derived from porphyritic rhyolites and rhyolitic ignimbrites of grayish color. The ignimbrite pebbles display a porphyritic texture and are composed of quartz, alkali feldspar, plagioclase and opaque minerals (magnetite and hematite, Fig. 4). Subhedral quartz of ~1.5 mm dimension is common, displaying corrosion edges as a consequence of reaction with the melt (Figs. 4B and F). Some crystals show a polycrystalline texture and contain feldspar inclusions. Alkali feldspars are perthitic sanidine crystals that are similar or larger in size than quartz (Fig. 4A) forming anhedral grains; Carlsbad-twinned indi-

viduals are common. Perthite exsolution textures are common, and show a weak, superficial argillic alteration. Small quartz crystals are dispersed in the matrix with rare, partially sericitized plagioclase. The matrix has developed a slightly banded flow structure. Previous shard glass is seen as an amoeboid recrystallized mosaic developed around phenocrysts. The matrix is partially altered to calcite and epidote. The size of magnetite is variable, and it has subhedral to anhedral crystal shapes.

The rhyolites with porphyritic textures were categorized into two groups according to the matrix:

1. A porphyritic texture group defined by perthitic sanidine phenocrysts, sericitized plagioclase, quartz and opaque minerals, in a fine-grained matrix (Fig. 4) (8061A). Sanidine crystals of ~ 1.5 mm have recrystallized to perthitic microcline with reabsorption edges displaying discontinuous twinning and perthitic texture. Anhedral plagioclase phenocrysts are rare and show fine polysynthetic twinning with incipient argillic alteration. Euhedral to subhedral quartz phenocrysts are noteworthy, with sizes up to 1.2 mm, and display evidence of reaction with melt along their borders. The equigranular matrix is represented by a mosaic of alkali feldspar and amoeboid quartz. Magnetite grains with polygon-like shapes are locally observed in the matrix. A weak post-magmatic alteration is defined by chlorite veinlets, fine white mica flakes and pistacite formation. The microcline is probably derived from sanidine and the transformation is due to the regional metamorphism which affected the rocks during the late Ediacaran to Early Cambrian.
2. A porphyritic texture defined by quartz and microcline phenocrysts in an aphanitic matrix (Fig. 4). Quartz is abundant as euhedral crystals with linear dimensions up to 2 mm; however, some quartz grains are anhedral probably due to reaction with the altered matrix. Alkali feldspar is represented by sanidine-microcline crystals of up 2.5 mm, displaying small twins or perthitic textures. The matrix is composed of equi-

**Fig. 3.** A: Combined probability density plots and histogram for detrital zircon ages from the Suncho Formation. Ages < 1000 Ma were calculated from the  $^{206}\text{Pb}/^{238}\text{U}$  ratios; and ages >1000 Ma from the  $^{207}\text{Pb}/^{206}\text{Pb}$  ratios (ADAMS et al. 2011). B: Zr/Ti vs. SiO<sub>2</sub> discrimination diagram of WINCHESTER & FLOYD (1977). The samples plot in the rhyolite field. C: Multi-element diagram normalized to C1 chondrite of SUN & McDONOUGH (1989), displaying negative anomalies of Rb, Nb, Sr and Y, typical for a volcanic arc and crustal genesis. D: Chondrite-normalized rare earth element diagram (SUN & McDONOUGH 1989), displaying the steep slope of the LREE, the negative Eu anomaly and the flat HREE. E: ACNK diagram [ $\text{Al}_2\text{O}_3 / (\text{CaO} + \text{Na}_2\text{O} + \text{K}_2\text{O})$ ] of SHAND (1929). The rhyolite samples plot in the metaluminous field. F: Rb vs. Y + Nb tectonic discrimination diagram of PEARCE et al. (1984). The samples plot in the volcanic arc granite (VAG) field.

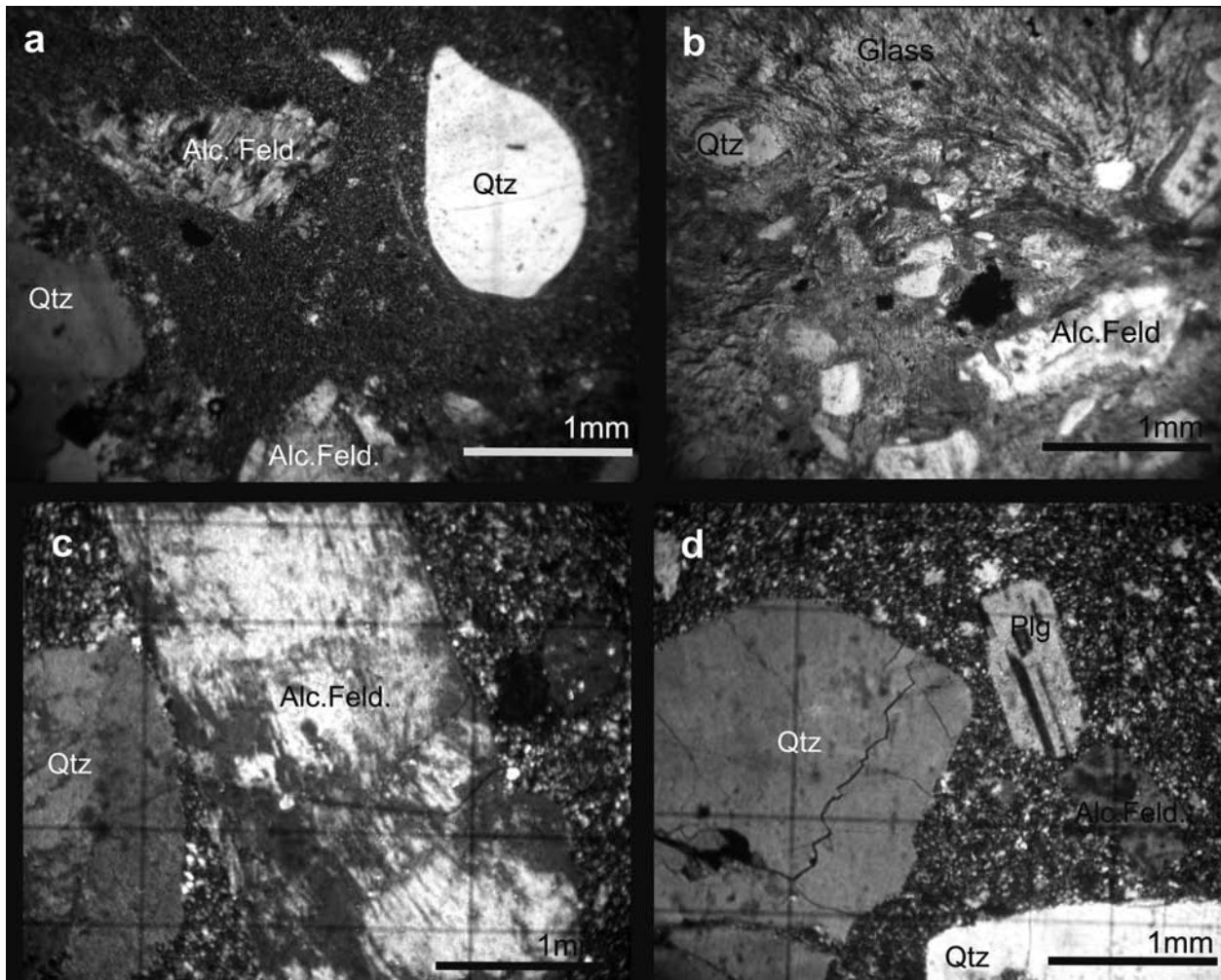


**Fig. 4.** Photomicrographs of rhyolite in thin section. **A** – Rhyolite with partly resorbed quartz and feldspars phenocrysts in an aphanitic matrix. **B** – Welded-tuff with development of vitreous-flow structures surrounded by recrystallized quartz and feldspar crystals. **C** – Rhyolite with xenocrysts of alkali-feldspar and anhedral quartz in an aphanitic matrix. **D** – Rhyolite with quartz, plagioclase and alkali-feldspar phenocrysts in a matrix of medium-grained quartz and feldspars.

granular microcrystalline crystals of quartz, feldspar and calcite, with few dispersed opaque minerals.

#### 4. Geochemical signatures

Major, minor and trace element concentrations of whole rock samples were determined at the Actlabs Laboratory (Canada; Table 1), using a standardized method that is a combination of lithium metaborate/tetraborate fusion and high precision INAA, ICP-WRA and ICP-MS determinations, using external standards of natural and synthetic materials for cali-

bration (detailed procedures at [www.actlabs.com](http://www.actlabs.com)).

The major element compositions of rhyolite samples 8061a and 8061b and ignimbrite 8090 were compared to average standards (e.g. LE MAITRE 1976; LOWER & CARMICHAEL 1970; MCBIRNEY 1984; LAGO et al. 1992).

Table 1 (see Appendix) shows that the rhyolite pebbles of the conglomerates in the Sierra de La Ovejería are higher in  $\text{SiO}_2$  (76.18 and 78.49%) than the averages. Concentrations of  $\text{TiO}_2$  (0.094 to 0.246%) and  $\text{Al}_2\text{O}_3$  (11.44 to 8.66%) are lower than the averages, and the meta-aluminous character of the samples is re-

flected by ACNK values ranging from 0.755 to 0.968 [ $\text{Al}_2\text{O}_3 / (\text{CaO} + \text{Na}_2\text{O} + \text{K}_2\text{O})$ ] (Fig. 3B). The alkali content ( $\text{Na}_2\text{O} + \text{K}_2\text{O} = 4.58$  to 5.91%) is similar to that of the standard and falls in the range of calc-alkaline series. The high concentration of CaO (1.96 to 2.79 wt%) are due to the carbonate and epidotic alteration described above.

The CIPW norm is shown in Table 1, indicating normative minerals quartz, albite, orthoclase and anorthite, and the accessory minerals are represented by magnetite, apatite and hematite. Normative diopside (in wollastonite and enstatite) is the result of the presence of secondary chlorite, calcite and epidote.

Abundances of trace elements such as Ba, Rb, Sr, Zr (ppm) are similar to the published standard values, but Y and Nb are depleted. Using the  $\text{Zr}/\text{TiO}_2$  vs.  $\text{SiO}_2$  classification diagrams of WINCHESTER & FLOYD (1977) (Fig. 3C), the samples are identified as rhyolites. Chondrite normalized rare earth elements (REE) are displayed in Fig. 3D (after SUN & McDONOUGH 1989). These display a remarkable negative Eu anomaly, indicating early plagioclase fractionation ( $\text{Eu}/\text{Eu}^* = 0.18$  to 0.25). The light REE (LREE) are weakly fractionated, and the HREE pattern is almost horizontal and gently concave [ $(\text{La}/\text{Yb})_{\text{N}} = 5.69$  to 9.28]. Total REE concentrations are remarkable high for this type of rocks (149.3 to 225.7 ppm)

Strong negative anomalies of incompatible elements (Rb, Sr, Y and Nb) in the chondrite normalized multi-element diagram (SUN & McDONOUGH 1989) suggest a volcanic arc origin for these samples. In addition, Th, U and Ta concentrations are very high (up to 30-900 times chondrite), whereas those of the heavy REE (HREE) and the high field-strength elements (HFSE) reach 20 times chondritic concentrations (Fig. 3E). These values are known to reflect fractional crystallization phenomena in shallow magmatic chambers. In the Rb vs.  $\text{Y}+\text{Nb}$  diagram of PEARCE et al. (1984) (Fig. 3F), the rhyolites fall in the volcanic arc field (VAG), but very close to the border with the within plate field (WPG).

#### 4.1. Analytical procedures and U-Pb zircon ages

The zircons were separated from ignimbrites and rhyolites and concentrated for analytical procedures at the Geosciences Institute of the São Paulo University (IGc/USP – Brazil). The samples were disintegrated to 100 and 250 mesh grain-sizes in a disc mill; the fragments then classified in a Wilfley table, and the fraction with heavy minerals was treated with bromo-

form and methyl iodide for separation. Concentrates were processed in a Frantz magnetic separator, and the final purification was carried out by hand picking under a stereomicroscope. Individual zircons selected for dating were mounted in epoxy resin. After polishing, reflected, transmitted and CL images were obtained to better choose the laser spot place (cathode luminescence) (Fig. 5A and B).

LA-ICP-MS analysis were carried out at the Geochronological Research Center, São Paulo University, Brazil, using a 193 nm excimer laser (Photon Machines) coupled to a Neptune multicollector, double-focusing magnetic sector ICP-MS. Operating procedures and parameters are discussed by SATO et al. (2011). Results are plotted on Tera Wasserburg diagrams (Fig. 5C, D and E) using Isoplot software (Ludwig et al. 2003). Using the “Concordia Age” model, the calculated zircon ages are  $524.9 \pm 1.1$  (MSWD = 0.47) and  $525.1 \pm 1.3$  Ma (MSWD = 0.038). These values were obtained considering only the best points after removing zircon xenocrysts that were incorporated into the magma, points with isotopic inheritance and analyses showing Pb loss. As the obtained ages are identical, we combined the data of both samples which provides an age of  $525.0 \pm 0.85$  Ma (MSWD = 0.44) (Fig. 5E). This is the best estimate for the age of formation of these volcanic rocks

#### 5. Magmatism and detrital zircon ages in the evolution of the Puncoviscana Basin

The Puncoviscana Basin developed during the Late Neoproterozoic and the Early Cambrian, encompassing an area from southern Bolivia to central Argentina. Further extension of the basin towards the north and south has also been suggested (ACEÑOLAZA & ACEÑOLAZA 2007; ACEÑOLAZA et al. 2009). The basin is interpreted as part of a western Gondwana shallow marine sedimentary basin receiving sedimentary input from older positive areas located to the north and east. This situation dramatically changed around 520 Ma, during the Tilcarian orogeny, which generated a major change in the sedimentary environment, with significant magmatic plutonic and volcanic influence.

Igneous rocks are common in northwest Argentina, with some remarkable units such as the Santa Rosa de Tastil granite, of which the red granite has a 541 Ma U-Pb zircon age, the gray granite a 534 Ma age, and a porphyritic dacite a 523 Ma age (HAUSER 2011). Westwards, near the town of Cachi in the Cordillera Oriental, LORK et al. (1990) obtained U-Pb ages for

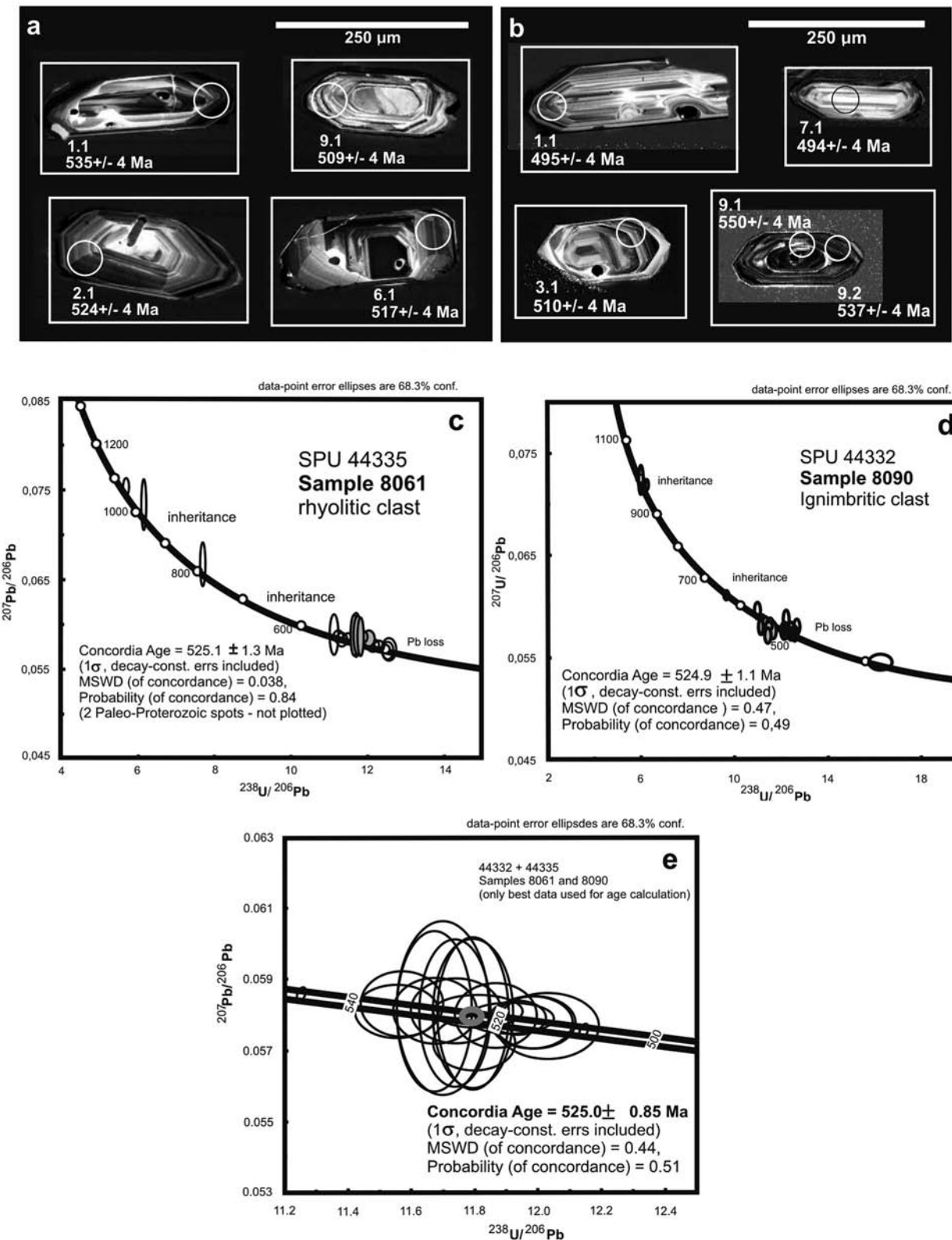


Fig. 5. A-B

volcanic detrital zircons in the range 530–560 Ma. The chemical and geochronological data from tuffs interbedded in the Puncoviscana Formation (ESCAVOLA et al. 2011) are very similar to those the rhyolite clasts presented herein. The abundance and distribution of interbedded tuffs in the Puncoviscana Formation and their chemical signatures highlight the importance of the regional magmatism and allows a close comparison with the rhyolite clasts in the Suncho Formation. Isotope geochemical data of rhyolite clasts indicate that the continental magmatic arc was active up to 515 Ma (HAUSER 2011; ESCAYOLA et al. 2011 and references therein) therefore we suggest that arc magmatism was related to the Tilcarian orogeny.

In addition, felsic magmatism was also reported from different areas in the Central Andean region, namely: (i) Sierra de Ambargasta in the Eastern Pre-cordillera (KOUKHARSKY et al. 2003) with volcanic series composed of rhyodacites, dacites, andesites and basaltic andesites having a 514 Ma K-Ar age and the geochemical characteristics of a continental volcanic arc; (ii) the Sierra Norte de Córdoba with magmatic arc related ignimbrites intercalated in conglomerates, with a 584 Ma conventional U-Pb age for magmatic zircons (LLAMBIA et al. 2003). Based on geochemical data, GOSSEN et al. (2009) suggested the succession formed in a continental island arc and were intercalated with sedimentary rocks during deposition in the same tectonic environment.

Although JEŽEK (1990) proposed a NE to E regional paleo-current direction, this is not clear for the Sierra de La Ovejería area. It is reasonable to assume that the volcanic outcrops containing the rhyolite clasts have been transported in the same direction (NE to E); however, we cannot rule out additional provenance from other regions.

## 6. Final remarks

The different lithofacies of the Suncho Formation and the nature and age of clasts in the conglomerate facies indicate that the sources were meta-sedimentary and

igneous rocks belonging to the Puncoviscana Formation and its intrusive rocks (Neoproterozoic–Terreneuvian, Series 2).

The presence of irregularly shaped, up to 6 cm long black limestone clasts within the conglomerates strongly suggests that carbonate sequences were part of an unknown, but nearby source area. The presence of limestones and the ages of the associated rhyolite clasts reinforce a regional link with outcrops in the Catamarca, Salta and Jujuy provinces. In addition, the rhyolite pebbles have a volcanic arc geochemical affinity.

On the basis of the regional paleocurrent patterns, the source area of the siliciclastic, carbonatic and volcanic material deposited in the Suncho Formation must have been located to the E and NE of the present outcrop.

Low temperature phases such as microcrysts, glassy and microcrystalline products indicate fast cooled effusive volcanism. Calc-alkaline and metaluminous rhyolites are common, characterizing evolved volcanic arcs. In addition, the ages and mineral compositions are similar to some of tuffs in the Puncoviscana Formation cropping out in the northern Salta and Jujuy provinces ( $515.1 \pm 5.9$  Ma and  $520.1 \pm 7.6$  Ma; ESCAYOLA et al. 2011).

The deposition of the Suncho Formation has a special significance in the geological tectonic evolution of the Lower Paleozoic of northwest Argentina and West Gondwana. The youngest detrital zircon U-Pb ages from the psammites display a noteworthy peak in the range 514–552 Ma. Some older ages found in the same unit (541–552 Ma) may correspond to the deeper sedimentary series that were sourced from magmatic rocks, while younger ages are related to the associated rhyolitic volcanism (514–520 Ma).

From the geochronological data of the Suncho Formation, we conclude that: 1) the age of sedimentation of the Suncho Formation cannot be greater than 525 Ma, which is the age of the vulcanite pebbles. 2) the sedimentary dynamics of the unit reflects reworking of the older Puncoviscana Formation (*sensu lato*). 3)

**Fig. 5. A–B** – Cathode luminescence images A – Zircons included from the rhyolites; B – Zircons from the ignimbrite. The circles indicate the analyzed points and are labelled with the corresponding ages. C – Tera-Wasserburg diagram for rhyolite zircons. Age:  $525.1 \pm 1.3$  Ma, with MSWD = 0.038 and a 0.84 probability of concordance. D – Tera-Wasserburg diagram for zircons from ignimbrite pebbles. Age:  $524.9 \pm 1.1$  Ma, with MSWD = 0.47 and a probability of 0.49. E – Tera-Wasserburg diagram for rhyolite and ignimbrite zircons. Combined age:  $525.0 \pm 0.85$  Ma, with MSWD = 0.44 and a 0.51 probability of concordance.

rhyolitic units belonging to early levels of the multi-phased Puncoviscana Formation, and were interlayered in the meta-sedimentary sequence of the source area. Its erosion produced the material for the Suncho Formation. 4) The ages obtained are consistent with those established by *Oldhamia* sp., included in the associated meta-sedimentary sequences. 5) The youngest detrital zircon ages of  $524.9 \pm 1$  and  $525.1 \pm 1.3$  Ma in the Suncho Formation were derived from acid volcanic rocks similar to that of the clasts in the conglomerates of the same unit. All data suggest a close affinity of the rhyolites with the tuffs levels described by ESCAYOLA et al. (2011) in the Puncoviscana Formation of the Salta and Jujuy provinces (523 and 569 Ma).

### Acknowledgements

Authors are indebted to STANLEY FINNEY and DIEGO GARCÍA-BELLIDO for field discussions and the early reading of manuscript. The reviewer's comments and suggestions greatly contributed to improve the final paper. Authors acknowledge the support from the Instituto Superior de Correlación Geológica (INSUGEO, Tucumán. Argentina) and the Centro de Pesquisas Geocronológicas (CpGeo, São Paulo. Brazil).

### References

- ACEÑOLAZA, F.G. & TOSELLI, A.J. (1978): Consideraciones petrográficas y tectónicas sobre el Paleozoico inferior del NW argentino. – 2<sup>nd</sup> Congreso Latinoamericano de Geología, **2**: 755-764.
- ACEÑOLAZA, G.F. & ACEÑOLAZA, F.G. (2007): Insights in the Neoproterozoic / early cambrian transition of NW Argentina: Facies, environments and fossils in the Proto Margin of Western Gondwana. – In: VICKERS-RICH, P. & KOMAROWER, P. (Eds.): The Rise and the Fall of the Ediacara Biota. – The Geological Society of London, Special Publication, **286**: 1-13.
- ACEÑOLAZA, G.F., GERMS, G. & ACEÑOLAZA, F.G. (2009): Trace fossils and the agronomic revolution at the Neoproterozoic – Cambrian transition in Southwest Gondwana. – Developments in Precambrian Geology, **16**: 339-347.
- ADAMS, C.J., MILLER, H., ACEÑOLAZA, F.G., TOSELLI, A.J. & GRIFFIN, W.L. (2011): The Pacific Gondwana margin in the late Neoproterozoic-early Paleozoic: Detrital zircon U-Pb ages from metasediments in northwest Argentina reveal their maximum age, provenance and tectonic setting. – Gondwana Research, **19**: 71-83.
- DURAND, F.R. (1980): Geología de la Sierra de La Ovejería, provincia de Catamarca. – PhD. Thesis (Facultad de Ciencias Naturales e Instituto Miguel Lillo, Universidad Nacional de Tucumán), pp. 1-365 (unpublished).
- DURAND, F.R. (1982): Caracteres geológicos del basamento de la Sierra de La Ovejería, Provincia de Catamarca. – Acta Geologica Lilloana, **16**: 93-109.
- DURAND, F.R. (1985): Caracterización geológica y paleoambiental de las psefitas de la Formación Suncho (Precámbrico Superior – Cámbrico Inferior). Provincia de Catamarca. – Acta Geologica Lilloana, **18**: 337-345.
- ESCAVOLA, M.P., VAN STAAL, C.R. & DAVIS, W.J. (2011): The age and tectonic setting of the Puncoviscana Formation in northwestern Argentina: An accretionary complex related to Early Cambrian closure of the Puncoviscana Ocean and accretion of the Arequipa-Antofalla block. – Journal of South American Earth Sciences, **32**: 438-459.
- GONZALEZ BONORINO, F. (1950): Geología y petrografía de la Hoja 12d (Capillitas) y 13d (Andalgalá). – Dirección General Industria y Minería, Boletín, **70**: 1-216.
- HAUSER, N. (2011): Petrología y geología isotópica de las rocas ígneas y estudios de proveniencia (U-Pb y Lu-Hf) de las rocas metasedimentarias del basamento del Paleozoico inferior en las áreas de Tastil, Niño Muerto, Río Blanco y Río Grande, Cordillera Oriental, Noroeste Argentino. – PhD. Thesis (Facultad de Ciencias Exactas y Naturales, Universidad Nacional de Salta), pp. 1-248 (unpublished).
- JEŽEK, P. (1990): Análisis sedimentológico de la Formación Puncoviscana entre Tucumán y Salta. – In: ACEÑOLAZA, F.G., MILLER, H. & TOSELLI, A.J. (Eds.): El Ciclo Pampeano en el Noroeste Argentino. – Serie Correlación Geológica, **4**: 9-35.
- KOUKHARSKY, M., BRODTKORB, M., KAY, S. & MUNIZAGA, F. (2003): La Formación Balbuena, integrante del arco magmático pampeano en la Sierra de Ambargasta, provincia de Santiago del Estero. – Revista de la Asociación Geológica Argentina, **58**: 583-592.
- LAGO, M., ALVARO, J., ARRANZ, E., POCOVÍ, A. & VAQUER, R. (1992): Condiciones del emplazamiento, Petrología y Geoquímica de las riolitas, calco-alcalinas y stephaniense-pérmicas, en las Cadenas Ibéricas. – Cuaderno Laboratorio Xeolóxico de Laxe, **17**: 187-198.
- LE MAITRE, R.W. (1976): The chemical variability of some common igneous rocks. – Journal of Petrology, **17**: 589-637.
- LLAMBÍAS, E., GREGORI, D., BASEI, M.A., VARELA, R. & PROZZI, C. (2003): Ignimbritas riolíticas neoproterozoicas en la Sierra Norte de Córdoba. Evidencia de un arco magmático temprano en el ciclo Pampeano? – Revista de la Asociación Geológica Argentina, **58**: 572-582.
- LORK, A., MILLER, H., KRAMM, U. & GRAUERT, B. (1990): Sistematica U-Pb de circones detriticos de la Formación Puncoviscana y su significado para la edad máxima de sedimentación en la Sierra de Cachi (Provincia de Salta, Argentina). – In: ACEÑOLAZA, F.G., MILLER, H. & TOSELLI, A.J. (Eds.): El Ciclo Pampeano en el Noroeste Argentino. Serie Correlación Geológica, **4**: 199-208.
- LOWDER, G.G. & CARMICHAEL, I.S.E. (1970): The volcanoes and caldera Talasea, New Britain: Geology and Petrology. – Bulletin of the Geological Society of America, **81**: 17-38.
- LUDWIG, K.R. (2003): Isoplot/Ex version 3.00. A Geochronological Toolkit for Microsoft Excel. – Berkeley Geochronology Center. Special Publication, **4**: 1-73.
- MCBIRNEY, A.R. (1984): Igneous Petrology. – Freeman Cooper & Co., pp. 1-509.
- MIRRÉ, J.C. & ACEÑOLAZA, F.G. (1972): El hallazgo de *Old-*

- hamia* sp. (traza fósil) y su valor como evidencia de edad cámbrica para el supuesto Precámbrico del borde occidental del Aconquija, provincia de Catamarca. – Ameghiniana, **9**: 72-78.
- PEARCE, J.A., HARRIS, N.B.W. & TINDLE, A.G. (1984): Trace element discrimination diagrams for the tectonic interpretation of granitic rocks. – Journal of Petrology, **25**: 956-983.
- RAPELA, C.W., PANKHURST, R.J., DAHLQUIST, J. & FANNING, C.M. (1999): U-Pb SHRIMP ages of Famatinian Granites: New constraints on the timing, origin and tectonic setting of I-and S-type magmas in an ensialic arc. – II South American Symposium on Isotope Geology (IIS-AGI), 264-267.
- SATO, K., BASEI, M.A.S., FERREIRA, C.M., SPROESSER, W.M., VLACH, S.R.F., IVANUCH, W. & ONOI, A.T. (2011): U-Th-Pb analyses by excimer laser ablation / ICP-MS on MG Brazilian xenotime. – Goldschmidt Conference Abstracts. – Mineralogical Magazine: 1801.
- SHAND, S.J. (1929): Eruptive Rocks. – D. Von Nostrand Co., New York, pp. 1-360.
- SUN, S.S. & McDONOUGH, W.F. (1989): Chemical and isotopic systematics of oceanic basalts: Implications for mantle composition and processes. – In: SAUNDERS, A.D. & NORRY, M.J. (Eds.): Magmatism in the Ocean Basins. Geological Society of London, Special Publication, **42**: 313-345.
- VON GOSEN, W., BUGGISCH, W. & PROZZO, C. (2009): Provenance and geotectonic setting of Latte Proterozoic-Early Cambrian metasediments in the Sierras de Córdoba and Guasayán (western Argentina): a geochemical approach. – Neues Jahrbuch für Geologie und Paläontologie, Abhandlungen, **25**: 257-284.
- WINCHESTER, W. & FLOYD, P.A. (1977): Geochemical discrimination of different magma series and their differentiation products using immobile elements. – Chemical Geology, **20**: 325-343.
- Manuscript received: June 2nd, 2014.  
Revised version accepted by the Potsdam editor: September 15th, 2014.
- Addresses of the authors:**
- DIMITRA MANTZOUKA, NICOLAOS TSAPARAS, VASILEIOS KARAKITSIOS, National and Kapodistrian University of Athens, Faculty of Geology and Geoenvironment, Department of Historical Geology and Palaeontology, Greece;  
e-mails: dmantzouka@geol.uoa.gr, ntsapar@geol.uoa.gr, vkarak@geol.uoa.gr,
- ALEJANDRO J. TOSELLI, Instituto Superior de Correlación Geológica (INSUGE - CONICET / Universidad Nacional de Tucumán). Miguel Lillo 205. 4000, Tucumán. Argentina.
- GUILLERMO F. ACEÑOLAZA (corresponding author), Instituto Superior de Correlación Geológica (INSUGE - CONICET / Universidad Nacional de Tucumán). Miguel Lillo 205. 4000, Tucumán. Argentina.  
e-mail: gfacenolaza@gmail.com
- FLORENCIO ACEÑOLAZA, Instituto Superior de Correlación Geológica (INSUGE - CONICET / Universidad Nacional de Tucumán). Miguel Lillo 205. 4000, Tucumán. Argentina.
- JUANA N. ROSSI, Instituto Superior de Correlación Geológica (INSUGE - CONICET / Universidad Nacional de Tucumán). Miguel Lillo 205. 4000, Tucumán. Argentina.
- MIGUEL A. BASEI, Centro de Pesquisas Geocronológicas (CPGeo), Instituto de Geociências, Universidade de São Paulo, Cidade Universitaria, Rua do Lago 562 (05508-900), São Paulo. Brasil.

## Appendix

**Table 1.** Major, trace and rare earth element concentrations and CIPW norms.

Sample	8061	8061b	8090
(oxide Wt%)			
SiO <sub>2</sub>	78.49	76.18	76.95
Al <sub>2</sub> O <sub>3</sub>	8.66	11.44	10.10
Fe <sub>2</sub> O <sub>3</sub> T	1.49	2.58	1.52
MnO	0.095	0.054	0.037
MgO	0.35	0.61	0.28
CaO	2.79	2.01	1.96
Na <sub>2</sub> O	2.57	3.13	3.31
K <sub>2</sub> O	2.01	2.78	2.59
TiO <sub>2</sub>	0.094	0.246	0.132
P <sub>2</sub> O <sub>5</sub>	0.03	0.06	0.02
LOI	3.09	1.66	2.16
Total	99.66	101.8	99.06
(ppm)			
Sc	3	6	3
V	8	25	9
Co	32	18	30
Ga	11	10	12
Rb	72	81	72
Sr	196	176	200
Y	31	27.6	31
Zr	114	210	161
Nb	18	11.5	18
Cs	3.7	3	4.3
Ba	506	785	737
Hf	4.5	5.9	5.6
Ta	4.3	2.97	4.1
Tl	0.3	0.4	0.4
Pb	79	17	30
Th	21.1	13.1	23.4
U	5.2	3.02	5.8
La	40.1	24.3	46.6
Ce	95.8	60.3	89.9
Pr	9.47	6.98	10.8
Nd	33.1	24.7	38.1
Sm	6.8	5.29	7.7
Eu	0.38	0.772	0.58
Gd	5.7	5.32	6.0
Tb	1.0	0.96	1.0
Dy	6.2	6.01	6.1
Ho	1.3	1.17	1.2
Er	3.6	3.36	3.5
Tm	0.56	0.499	0.53
Yb	3.8	3.06	3.6
Lu	0.63	0.464	0.57
Eu/Eu*	0.18	0.44	0.25
La/Yb)N	7.57	5.69	9.28
<b>CIPW norms</b>			
	8061	8061b	8090
Q	54.40	42.83	46.24
Or	12.31	16.59	15.81
Ab	22.49	26.70	28.87
An	6.32	9.01	5.19
Di -Wo	1.05	0.30	0.84
Di -En	0.91	0.25	0.72
Hy -Ms	-	1.28	-
Mt	0.04	0.18	0.12
He	1.52	2.48	1.48
Ap	0.07	0.13	0.05

**Table 2. A.** Best quality U-Pb data used for age calculation.

SPU	Fraction	207/235	Error (ls)	206/238	Error (ls)	Coef. corr.	238/206	Error (ls)	207/206	Error (ls)	208/206	Error (ls)	T206/238	Error (ls)	T207/206	Error (ls)	%Conc.
44332	1.1	0.6879	0.0063	0.0865	0.0007	0.83	11.556	0.0879	0.0851	0.0005	0.3215	0.0948	0.535	0.004	0.528	0.019	101
44332	4.1	0.6999	0.0097	0.0864	0.0006	0.52	11.571	0.0845	0.0853	0.0006	0.3279	0.0988	0.534	0.004	0.536	0.024	100
44332	5.1	0.6785	0.005	0.085	0.0006	0.86	11.7669	0.0897	0.0858	0.0005	0.1327	0.0402	0.526	0.004	0.524	0.019	100
44332	6.1	0.6657	0.0063	0.0835	0.0006	0.77	11.979	0.0874	0.0578	0.0005	0.2896	0.088	0.517	0.004	0.516	0.020	100
44332	10.1	0.6839	0.0067	0.0857	0.0006	0.75	11.6727	0.086	0.0581	0.0006	0.3085	0.0906	0.530	0.004	0.529	0.024	100
44332	12.1	0.6662	0.0062	0.0843	0.0006	0.76	11.8673	0.084	0.058	0.0006	0.1652	0.0521	0.522	0.004	0.523	0.021	100
44332	15.1	0.6647	0.0078	0.0839	0.0006	0.64	11.9137	0.0894	0.0579	0.0003	0.2357	0.0866	0.520	0.004	0.519	0.012	100
44332	19.1	0.6679	0.0085	0.0834	0.0006	0.56	11.9861	0.0851	0.0578	0.0005	0.2389	0.1001	0.517	0.004	0.516	0.020	100
44332	23.1	0.6751	0.0074	0.0848	0.0006	0.65	11.7977	0.0839	0.0581	0.0003	0.2541	0.1040	0.524	0.004	0.526	0.012	100
44332	24.1	0.6742	0.0072	0.0846	0.0006	0.65	11.8298	0.0824	0.0584	0.0003	0.0543	0.0226	0.523	0.004	0.526	0.010	100
44332	2.1	0.6605	0.0057	0.0848	0.0006	0.84	11.7987	0.0864	0.0572	0.0005	0.2483	0.0736	0.524	0.004	0.494	0.020	106
44335	4.1	0.6536	0.0091	0.0831	0.0007	0.62	12.029	0.1037	0.0577	0.0006	0.3395	0.0483	0.515	0.004	0.513	0.024	100
44335	6.1	0.6774	0.0081	0.0842	0.0006	0.64	11.882	0.0915	0.0579	0.0004	0.1789	0.0521	0.521	0.004	0.521	0.016	100
44335	12.1	0.6767	0.0094	0.0851	0.0007	0.59	11.7462	0.0965	0.0581	0.0006	0.1560	0.0239	0.527	0.004	0.528	0.022	100
44335	13.1	0.6833	0.0168	0.0855	0.0007	0.33	11.7026	0.0951	0.0582	0.0016	0.2863	0.0631	0.529	0.004	0.530	0.058	100
44335	17.1	0.6777	0.0149	0.0853	0.0005	0.29	11.7295	0.0753	0.0581	0.0014	0.0447	0.0093	0.527	0.003	0.528	0.053	100
44335	20.1	0.6858	0.0151	0.0857	0.0006	0.29	11.669	0.0750	0.0581	0.0015	0.2260	0.0433	0.530	0.003	0.528	0.054	100
44335	22.1	0.6734	0.0145	0.0846	0.0005	0.27	11.8205	0.0695	0.0580	0.0014	0.1776	0.0328	0.524	0.003	0.524	0.052	100
44335	24.1	0.6852	0.0148	0.0848	0.0005	0.29	11.795	0.0731	0.0580	0.0014	0.8544	0.1522	0.525	0.003	0.523	0.053	100

**Table 2 B.** Neoproterozoic or older inheritance.

SPU	Fraction	207/235	Error (ls)	206/238	Error (ls)	Coef. corr.	238/206	Error (ls)	207/206	Error (ls)	208/206	Error (ls)	T206/238	Error (ls)	T207/206	Error (ls)	%Conc.
44332	16.1	0.7042	0.0091	0.0911	0.0007	0.64	10.9746	0.0863	0.0596	0.0005	0.26	0.0968	0.562	0.004	0.582	0.019	97
44332	3.1	1.6005	0.0213	0.1762	0.0018	0.81	5.9798	0.0643	0.0724	0.0009	0.7933	0.2363	0.997	0.01	0.997	0.025	100
44332	21.1	1.6032	0.0169	0.1611	0.0011	0.63	6.2092	0.0415	0.0720	0.0003	0.9638	0.3833	0.963	0.006	0.987	0.01	98
44332	25.1	0.8739	0.0096	0.1038	0.0007	0.64	9.6328	0.0675	0.0611	0.0003	0.3055	0.1286	0.637	0.004	0.637	0.012	100
44335	9.1	0.7108	0.0086	0.0891	0.0007	0.63	11.2254	0.0847	0.0587	0.0004	0.909	0.0141	0.655	0.004	0.548	0.016	100
44335	9.2	0.7009	0.0081	0.0869	0.0006	0.64	11.5123	0.0854	0.0584	0.0004	0.1507	0.0223	0.537	0.004	0.539	0.015	102
44335	11.1	0.7138	0.009	0.0883	0.0007	0.61	11.3278	0.0877	0.0583	0.0005	0.1767	0.0266	0.545	0.004	0.533	0.017	100
44335	14.1	0.7294	0.0163	0.090	0.0009	0.32	11.1153	0.0783	0.0589	0.0015	0.2592	0.0557	0.555	0.004	0.558	0.054	100
44335	23.1	1.1961	0.0251	0.1302	0.0009	0.31	7.6824	0.0507	0.0667	0.0016	0.2396	0.0433	0.789	0.005	0.824	0.05	96
44335	19.1	1.637	0.0347	0.1625	0.001	0.30	6.1554	0.0397	0.0734	0.0018	0.4682	0.0903	0.970	0.006	1.025	0.049	95
44335	10.1	1.8366	0.0224	0.1757	0.0014	0.64	5.6903	0.0447	0.0754	0.0006	0.1617	0.0243	1.044	0.008	1.08	0.016	97
44335	18.2	11.0302	0.0243	0.14396	0.0026	0.27	2.2749	0.0134	0.1827	0.0046	0.2408	0.0474	2.349	0.012	2.68	0.042	88
44335	18.1	11.496	0.2651	0.4837	0.003	0.27	2.0590	0.0128	0.1745	0.0044	0.1330	0.0267	2.552	0.013	2.601	0.043	98

**Table 2 C.** Different degrees of Pb loss.

SPU	Fraction	207/235	Error (ls)	206/238	Error (ls)	Coef. corr.	238/206	Error (ls)	207/206	Error (ls)	208/206	Error (ls)	T206/238	Error (ls)	T207/206	Error (ls)	%Conc.
44332	14.1	0.6591	0.0074	0.0822	0.0006	0.60	12.1705	0.0828	0.0577	0.0003	0.1066	0.0387	0.509	0.003	0.511	0.012	100
44332	17.1	0.6277	0.0080	0.0799	0.0006	0.63	12.5092	0.1000	0.0573	0.0004	0.2215	0.0835	0.496	0.004	0.498	0.014	100
44332	18.1	0.6415	0.0075	0.0804	0.0006	0.63	12.4455	0.0924	0.0573	0.0003	0.4246	0.0922	0.493	0.004	0.497	0.013	100
44332	20.1	0.6216	0.0078	0.0795	0.0006	0.62	12.5766	0.0972	0.0573	0.0005	0.2728	0.1071	0.493	0.004	0.496	0.017	100
44332	22.1	0.6376	0.0074	0.0811	0.0006	0.63	12.3271	0.0896	0.0574	0.0004	0.114	0.0461	0.503	0.004	0.501	0.015	100
44332	7.1	0.6373	0.0054	0.0791	0.0006	0.84	12.6458	0.0899	0.0580	0.0005	0.0708	0.0217	0.491	0.003	0.524	0.019	94
44332	11.1	0.6693	0.0061	0.0819	0.0006	0.77	12.2026	0.0861	0.0587	0.0006	0.3339	0.1044	0.508	0.003	0.551	0.022	92
44332	3.2	0.4470	0.012	0.0615	0.0013	0.82	16.2524	0.3563	0.0546	0.0005	0.197	0.385	0.008	0.003	0.390	0.022	99
44335	2.1	0.6431	0.0094	0.081	0.0007	0.55	12.3392	0.0999	0.0574	0.0006	0.2189	0.0308	0.502	0.004	0.502	0.024	100
44335	3.1	0.6463	0.0084	0.0823	0.0007	0.63	12.1476	0.0986	0.0577	0.0005	0.2978	0.0293	0.510	0.004	0.512	0.018	100
44335	5.1	0.6559	0.0080	0.0812	0.0006	0.61	12.3129	0.0919	0.0576	0.0004	0.2006	0.0287	0.503	0.004	0.510	0.016	99
44335	8.1	0.6373	0.0094	0.0809	0.0008	0.68	12.3555	0.1229	0.0575	0.0005	0.1497	0.0219	0.502	0.005	0.503	0.018	100
44335	21.1	0.6374	0.0168	0.0817	0.0006	0.30	12.2397	0.0964	0.0571	0.0016	0.2507	0.0472	0.506	0.004	0.507	0.061	100
44335	1.1	0.6520	0.0091	0.0798	0.0006	0.57	12.5351	0.0997	0.0571	0.0008	0.3648	0.0509	0.495	0.004	0.488	0.022	101
44335	7.1	0.6276	0.0104	0.0797	0.0007	0.57	12.5547	0.1178	0.0572	0.0008	0.3171	0.0468	0.494	0.004	0.492	0.029	100

